Volume 2 | Number 4 | 28 January 2014 | Pages 335–444

Journal of Materials Chemistry B

Materials for biology and medicine

www.rsc.org/MaterialsB

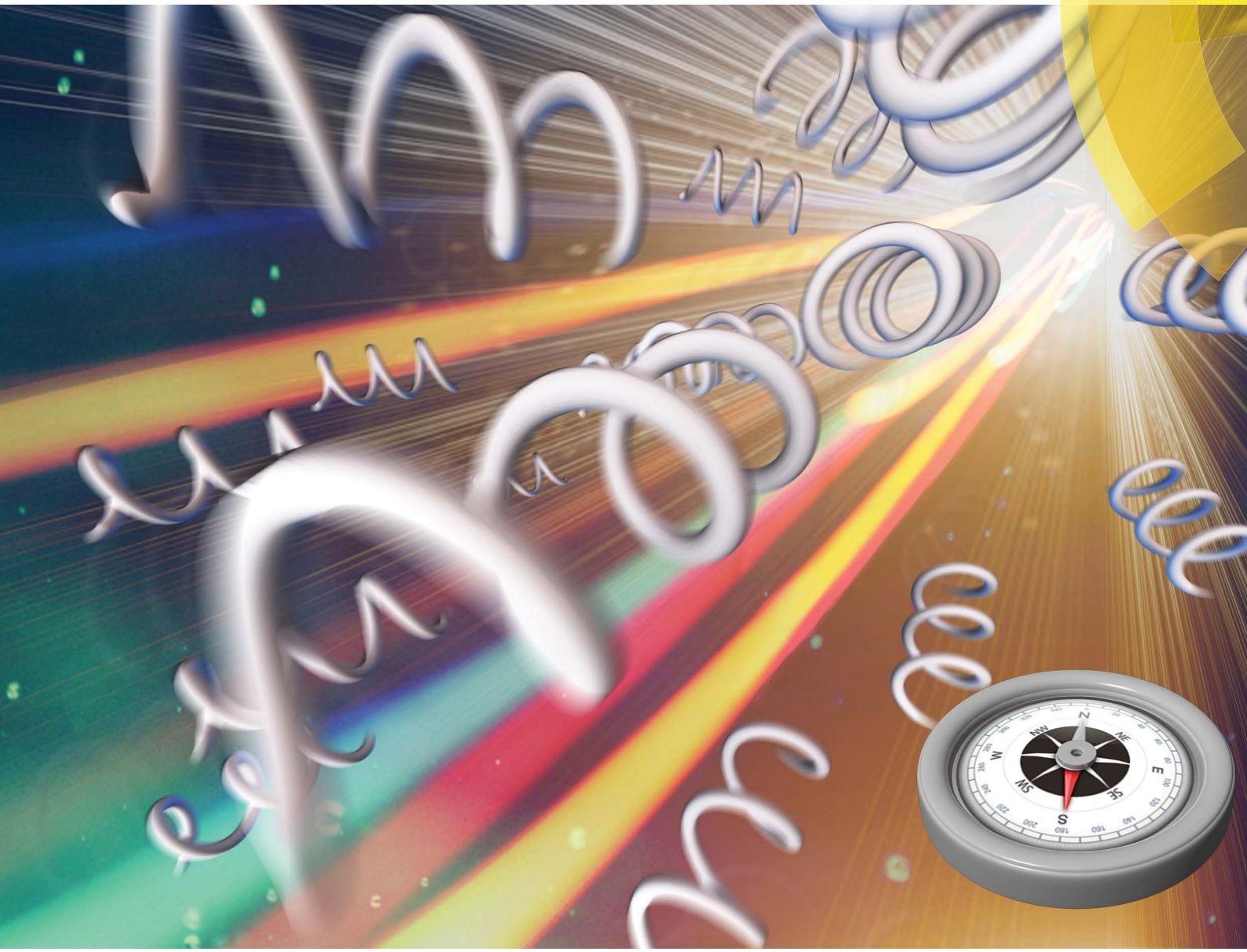

ISSN 2050-750X

ROYAL SOCIETY OF CHEMISTRY

PAPER

Bradley J. Nelson *et al.*

Noncytotoxic artificial bacterial flagella fabricated from biocompatible ORMOCOMP and iron coating

Journal of Materials Chemistry B

PAPER

View Article Online
View Journal | View Issue

Cite this: J. Mater. Chem. B, 2014, 2, 357

Noncytotoxic artificial bacterial flagella fabricated from biocompatible ORMOCOMP and iron coating†

Famin Qiu,[a] Li Zhang,[b] Kathrin E. Peyer,[a] Marco Casarosa,[c] Alfredo Franco-Obregón,[cd] Hongsoo Choi[e] and Bradley J. Nelson*[a]

Received 13th June 2013
Accepted 12th November 2013

DOI: 10.1039/c3tb20840k

www.rsc.org/MaterialsB

Magnetic microrobots have potential use in biomedical applications such as minimally invasive surgery, targeted diagnosis and therapy. Inspired by nature, artificial bacterial flagella (ABFs) are a form of microrobot powered by magnetic helical propulsion. For the promise of ABFs to be realized, issues of biocompatibility must be addressed and the materials used in their fabrication should be carefully considered. In this work, we fabricate the helical bodies of ABFs from a commercially available biocompatible photoresist, ORMOCOMP, by subsequently coating them with Fe for magnetic actuation. 3-(4,5-Dimethylthiazol-2-yl)-2,5-diphenyltetrazolium bromide (MTT) assays show that Fe-coated ORMOCOMP layers do not undermine the cell viability during 72 hours of incubation compared to control substrates. Cells exhibit normal morphology on ABF arrays and show good lamellipodial and filopodial interactions with the ABF surfaces. The swimming performance of Fe-coated ABFs is characterized using a three-pair Helmholtz coil arrangement. ABFs exhibit a maximum forward speed of 48.9 μm s^{-1} under a field of 9 mT at a frequency of 72 Hz. In summary, our Fe-coated ABFs exhibit little cytotoxicity and have potential for *in vivo* applications, especially those involving difficult to access regions within the human body.

Introduction

Nano-/microrobots powered by magnetic fields can be used in biomedical applications requiring minimally invasive surgery, targeted diagnosis and therapy, because of their ability to be remotely controlled by wireless means using low magnetic fields that are innocuous to cells and tissues.[1–11] Artificial bacterial flagella (ABFs) are one kind of helical microrobot inspired by nature. They possess a helical shape and are composed of magnetic materials. By mimicking the propulsion mechanics of bacterial flagella,[12] they can perform three-dimensional navigation in liquid with a wide range of viscosities such as water, blood, fetal bovine serum (FBS) and urine by translating rotational moment into forward propulsion. Helical propulsion has proven to be one of the most promising methods for biomedical applications, especially *in vivo* applications such as targeted drug delivery.[2,13–15]

fabrication section

The first ABF was reported in 2007.[16] The fabrication process was based on thin-film deposition and self-scrolling technology.[17,18] It consisted of a helical "tail" composed of an InGaAs/GaAs bilayer and a Ni magnetic "head" for actuation. Zhang *et al.* in 2009 used a similar method of fabrication to produce ABFs with the addition of a Cr layer between the "head" and the "tail" to improve adhesion.[19] Their magnetic actuation was investigated,[20,21] subsequently, the ability of the fluid flow generated by their swimming motion to manipulate micro-objects was demonstrated.[22,23] Recent ABFs reported by Tottori *et al.* used 3D laser direct writing (DLW) and e-beam deposition.[24] Helical shapes were directly fabricated in negative photoresists with Ni/Ti bilayer coating or magnetic polymer composites (MPCs) using two-photon polymerization (TPP).[25–27] The helical microswimmers performed precise corkscrew motion in FBS and DI water. Cargo transport and the release of microparticles in 2D and 3D were demonstrated.[24]

For biomedical applications the biocompatibility of ABFs is imperative.[28] The materials for building these devices must be carefully chosen. ORMOCOMP, a member of the ORMOCER® family, is a commercially available gel resist composed of inorganic–(Si–O–Si)–organic groups.[29,30] While the detailed

[a]Institute of Robotics and Intelligent Systems, ETH Zurich, Zurich, CH-8092, Switzerland. E-mail: bnelson@ethz.ch

[b]Department of Mechanical and Automation Engineering, The Chinese University of Hong Kong, Hong Kong SAR, China

[c]Institute for Biomechanics, ETH Zurich, Zurich, CH-8093, Switzerland

[d]Department of Surgery, Yong Loo Lin School of Medicine, National University of Singapore, Singapore

[e]Robotics Engineering Department, Daegu Gyeongbuk Institute of Science and Technology (DGIST), 711-873, Daegu, South Korea

† Electronic supplementary information (ESI) available: Video S1 shows DLW writing of helices in photoresist in real time. Video S2 shows an Fe-coated ABF moving in DI-water under 9 mT at 72 Hz. The controlled swimming is also shown. See DOI: 10.1039/c3tb20840k

chemical composition of ORMOCOMP is proprietary, previous results have shown that ORMOCOMP is biocompatible, and supports cell proliferation, viability and normal morphology of various cell lines.[29,31,32] Growing interest in ORMOCOMP in biomedicine and tissue engineering exists,[31,33] where hollow microneedles for transdermal drug delivery[32,34] and elastic three-dimensional scaffolds for single-cell force measurements have been developed.[30,35]

The actuation of our ABFs requires magnetic materials. Ni, Fe, Co and their alloys are soft magnetic materials often used for microscale structures because of their compatibility with surface deposition methods such as physical vapor deposition (PVD) and electro-deposition methods. These metals readily conform to irregular topographies compared to other permanent magnetic materials. Ni and Co, however, are cytotoxic.[36] On the other hand, pure iron can be biocompatible and biodegradable.[37–39]

In this paper, the biocompatible photoresist ORMOCOMP was used to fabricate the helical shapes using TPP technology, while Fe thin films were coated on the helical polymeric bodies for magnetic actuation. The fabrication results were validated by using a scanning electron microscope (SEM). Cell viability was tested by 3-(4,5-dimethylthiazol-2-yl)-2,5-diphenyltetrazolium bromide (MTT) assays, and the morphology of cells interacting with ABFs was demonstrated by SEM. The swimming performance of ABFs was characterized by a three-pair Helmholtz coil setup.

Results and discussion

Fabrication of ABFs

Fig. 1 shows the fabrication process (Fig. 1a and b) and the SEM image (Fig. 1c) of arrays of ABFs. The mean length and diameter of one helix are 15.7 μm and 5.3 μm, respectively (the inset of Fig. 1c), and are highly reproducible. A single helix can be produced every 2.3 s at a writing speed of 25 μm s^{-1}, although the fabrication time can be shortened by increasing the writing speed (see the Experimental section for a more detailed description). Another biocompatible photoresist SU-8 has also been used to fabricate helical microstructures using TPP.[24] Compared to SU-8, ORMOCOMP alleviates the need for spin-coating and pre-backing steps, thus, saving the fabrication time. ORMOCOMP also has better cell curability in biomedical applications,[31,40] as it does not require further surface modifications such as O_2 plasma treatment and chemical treatment, as does SU-8 due to its hydrophobicity.[40] After the fabrication of helical arrays from ORMOCOMP, Fe (25 nm) or Fe/Ti (25 nm/15 nm) thin films were coated onto the bodies by electron beam deposition. We refer to "Fe–ABFs" and "FeTi–ABFs" to represent Fe-coated ABFs and Fe/Ti-coated ABFs, respectively.

Cell viability of ABFs

To determine the biocompatibility of the materials used to fabricate Fe–ABFs and FeTi–ABFs, cell viability was assayed on two-dimensional surfaces coated with ORMOCOMP/Fe or ORMOCOMP/Fe/Ti layers by MTT, as previously described.[41]

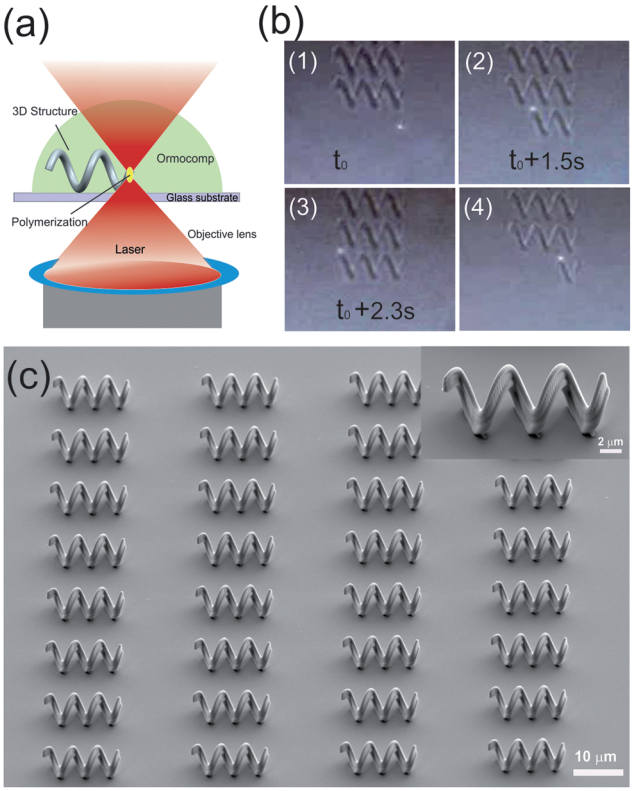

Fig. 1 Fabrication of helical structures using Direct Laser Writing (DLW). (a) Schematic of writing a helix in the ORMOCOMP photoresist. The photoresist present at the laser focal point polymerizes based on two-photon-polymerization. The 3D helical structure is written by moving the laser focus point in a helical path. (b) The real time writing process of helical structures. The bright point is the laser focus point. From (1) to (3), a helix was finished, then the laser focus point moves to the next defined position to write another helix (picture (4)). (c) SEM images of an array of helical microstructures. The inset is a magnification of a single helix.

Fig. 2a shows MTT results of C2C12 mouse myoblasts grown on distinct substrates after 24, 48 and 72 hours. The MTT test detects the reduction of MTT (yellow) to MTT formazan (purple) within the mitochondria of living cells, a measure of cell respiratory capacity, and hence, is widely used to measure cell viability, proliferation and cytotoxicity.[36,42–45] By comparing the optical intensity of formazan between cells grown on control Fe and Ti substrates (Fig. 2b), we obtained a measure of cytotoxicity of the distinct components. Clean glass substrates served as the reference (control) condition.[29] Fig. 2a shows that the cell compatibility of the ORMOCOMP/Fe film is somewhat lower than that of clean glass (control) after 24 hours of incubation, whereas SEM images (Fig. 2c) do show that cells spread and make functional membrane contacts on the ORMOCOMP/Fe surface at this time point. Indeed, ORMOCOMP/Fe/Ti appears to enhance the cell viability after 72 hours of incubation, as previously described for rat myoblasts on titanium containing structures.[46] We also conducted MTT assays on substrates that were never exposed to cells to test for the possibility that these materials might produce a MTT signal on their own after 72 hours of incubation (Fig. S1†). None of these materials

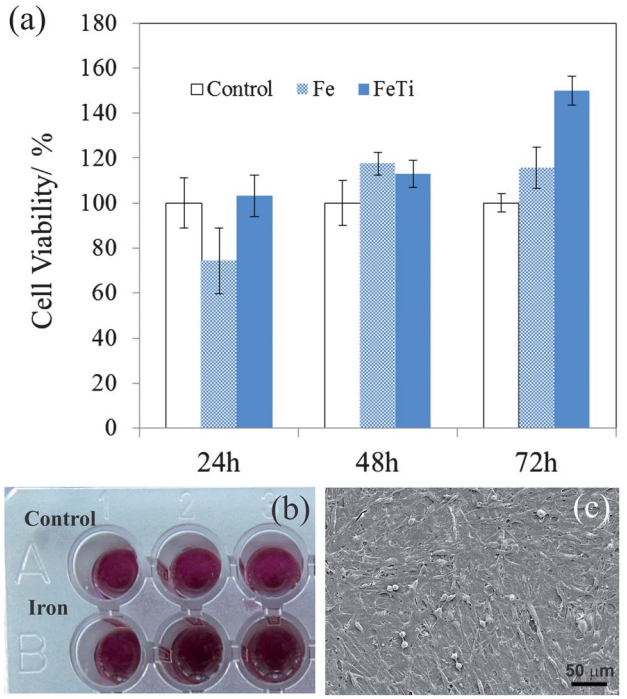

Fig. 2 Cell viability of Fe–ABFs and FeTi–ABFs. (a) MTT tests of cell viability for C2C12 mouse muscle cells cultured on clean glasses (showed as 'control'), ORMOCOMP coated glasses with a Fe metal layer (showed as 'Fe'), and ORMOCOMP coated glasses with Fe/Ti layers (showed as 'FeTi') after incubation of 24 hours, 48 hours and 72 hours, respectively. The optical intensities were normalized to the intensities of the control. The error bars show the standard deviation of mean values where $n = 8$. (b) Optical image of MTT results after two-day incubation. (c) Cells spread on the entire ORMOCOMP/Fe surface after seeding (2.5×10^5 cells per ml) for 24 hours.

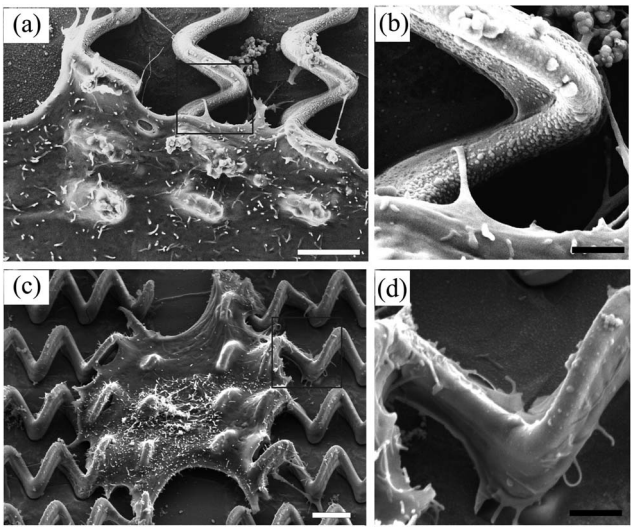

Fig. 3 Morphology of cells on Fe–ABFs and FeTi–ABFs after 24 hours of incubation. (a) Cells on Fe–ABFs, (b) magnified image of the rectangular area shown in (a), (c) cells on FeTi–ABFs, and (d) magnified image of the rectangular area shown in (c). The white scale bar in (a) and (c) is 4 μm, and the black scale bar in (b) and (d) is 1 μm.

produced a sufficient amount of MTT formazan to invalidate our initial result.

Morphology of cells on ABFs

The MTT assays performed in this work show that the ORMOCOMP/Fe and ORMOCOMP/Fe/Ti films are not cytotoxic to mammalian muscle cells, representing the predominant tissue mass in the body. Another method to monitor the viability of cells is to examine their interactions with their surroundings. Healthy cells are more proliferative, which require focal adhesion contacts with their substrates recruiting dynamic lamellipodial and filopodial attachment and retractions. Fig. 3 shows C2C12 cells contacting and spreading on Fe–ABFs (Fig. 3a) and FeTi–ABFs (Fig. 3c) with lamellipodial and filopodial interactions of normal morphology.[2,24,28]

Iron is oxidized in an aqueous biological environment. Once the Fe coating is degraded the ABFs will lose their swimming functionality which is driven by magnetic actuation. Fig. 3b shows a portion of an ABF with the surface roughened due to the corrosion of the exposed iron surface in physiological saline.[47] By contrast, Fig. 3d shows the comparably smooth surface of an ABF whose iron surface was coated by a thin (15 nm) coating of Ti that is highly resistant to corrosion.[48] Hence, the functional life-time of ABFs may be extended for *in vivo* applications by coating the surface of Fe–ABFs with anti-corrosive Ti.

Our experiments were conducted *in vitro*. A previous study by Waksman *et al.* demonstrated the safety of iron stents (10 mm in length) in porcine coronary arteries after 28 days with no evidence of embolization, thrombosis, excess inflammation or fibrin deposition.[49] Furthermore, Peuster *et al.* studied the long-term biocompatibility of iron stents (20 mm in length) in the porcine descending aorta for 360 days and showed no evidence for local toxicity due to corrosion products adjacent to the iron stent.[39] They claimed iron is a suitable metal for large-size degradable stents with no local or systemic toxicity. We can, therefore, assume that our Fe–ABFs, which are three orders of magnitude smaller than the iron stents, should be safe *in vivo* and maintain functionality. Another advantage of iron for *in vivo* applications is its micronutrient value for normal metabolism that is required for efficient systemic gas exchange and mitochondrial function.[49]

Swimming performance of ABFs

Fig. 4a shows the forward velocity of Fe–ABFs and FeTi–ABFs as a function of input frequency driven by two magnetic fields with strengths of 1 mT and 3 mT. The swimming tests were conducted immediately after Fe coating and Fe/Ti coating. The curves show that the forward speed of Fe–ABFs and FeTi–ABFs increases with increasing input frequency below a critical value called the step-out frequency, the maximum magnetic field frequency that the ABFs can follow synchronously.[13,20,22,50] When the applied magnetic field frequency exceeds the step-out frequency, the forward speed of ABFs drops dramatically. The step-out frequency increases with the strength of the magnetic fields. When the magnetic field increased from 1 mT

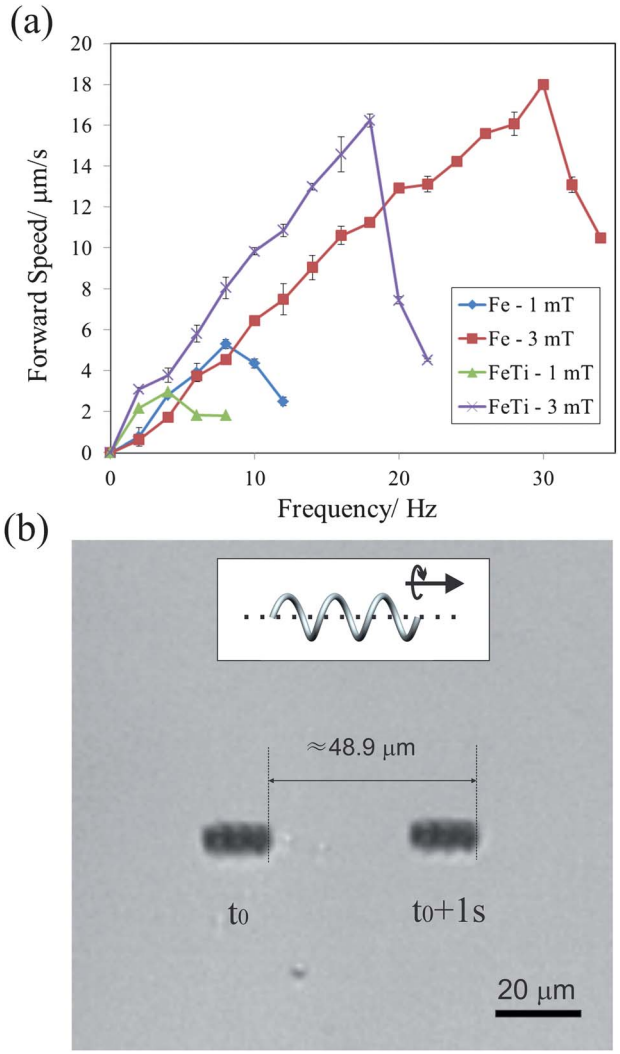

Fig. 4 Swimming behaviors of Fe–ABFs and FeTi–ABFs. (a) Forward velocities of Fe–ABFs and FeTi–ABFs as a function of frequency under two different field strengths of 1 mT and 3 mT. The error bars represent the standard deviations of mean values from three measurements at each frequency. (b) The swimming performance of an Fe–ABF under 9 mT at 72 Hz. All swimming tests were conducted in DI-water.

to 3 mT, the step-out frequency of Fe–ABFs increased from 8 Hz to 28 Hz. The maximum swimming speed increased from 5.3 μm s^{-1} to 18.0 μm s^{-1}. When driven by higher magnetic fields and higher frequencies, ABFs achieve higher speeds. The maximum forward speed of Fe–ABFs was 48.9 μm s^{-1} (3.1 body lengths per second) at a field strength of 9 mT under 72 Hz (Fig. 4b and Video S2,† the video also shows the controlled actuation of an Fe-coated ABF). After coating Ti, the maximum speed of ABFs under 1 mT and 3 mT slightly decreases compared to Fe–ABFs due to the additional weight of nonmagnetic Ti. We assume that by increasing the thickness of magnetic Fe coating and improving the design, the speed of ABFs can increase further. For example, our previous work showed that helical swimmers (8 μm in diameter, 35 μm in length) with 100 nm Ni coating attain the highest speed of 320 μm s^{-1} in DI water.[24]

Conclusions

Iron-coated ABFs were fabricated from biocompatible ORMOCOMP using TPP and e-beam deposition methods. Viability assessment and SEM imaging of the cell interaction with ABFs reveal little cytotoxicity for up to three days in culture. The Fe–ABF swimmers have a maximum forward velocity of 48.9 μm s^{-1} under 9 mT. Our noncytotoxic ABF microdevices can be precisely controlled by low-strength magnetic fields and have great potential to be used for *in vivo* targeted drug delivery. Furthermore, the fabrication methods (TPP methods combined with e-beam deposition) and chosen materials open a door for achieving other noncytotoxic magnetic microdevices. Future innovation will involve the functionalization of ABFs with drugs for biomedical applications such as targeted drug delivery.

Experimental section

DLW of helical polymeric bodies

ORMOCOMP (Micro resist technology GmbH) was coated on the clean glass substrate by a droplet. The 3D helices were then written in the resist using a Nanoscribe (from Nanoscribe GmbH) with the oil-immersion 100× objective (NA = 1.4 from Zeiss, NA denotes numerical aperture). The two important writing parameters, laser power and scan speed, were 5 mW and 25 μm s^{-1}, respectively. The fabrication process of iron-based ABFs can be divided into two steps: the first step is to fabricate helical polymer bodies in ORMOCOMP using 3D direct laser writing based on two-photon polymerization principle. The laser beam was focused by an objective lens in the photoresist. The volume at the focal point polymerizes from a gel to a solid, and a piezo stage drives the laser focal point in a designed 3D pattern to form helices. Fig. 1a shows the scheme of writing a helix in the ORMOCOMP photoresist. Fig. 1b shows how helices were written in the gel photoresist, (1) shows the machine starting to write a helix, (3) shows a helix written, and (4) shows the laser focal point moved to another new defined position to write a new helix (Video S1† shows real-time writing of helices in the photoresist). Two-minute post bake at 80 °C was followed after writing. The sample was immersed in an Ormodev developer (from micro resist technology GmbH) for 7 minutes to remove the un-polymerized resist and rinsed in isopropanol (IPA) immediately followed by gentle nitrogen blow.

Deposition of metals

Fe and Ti thin films were deposited using electron beam deposition with a rotational speed of 10–15 rpm. The tilt angle for deposition was 15° in order to reduce the shadowing effect.[24] The deposition rate was 0.6–2 Å s^{-1}.

Preparation of samples for the MTT test

The MTT test was used to check the cell viability of ORMOCOMP/Fe and ORMOCOMP/Fe/Ti layers. A thin layer of ORMOCOMP was spin-coated on a clean glass substrate with a diameter of 12 mm, and Fe or Fe/Ti layers were deposited on the

ORMOCOMP layer by e-beam deposition to mimic the material composition of ABFs.

MTT assays

Cell substrates were sterilized in 10% penicillin–streptomycin (from PAA) in phosphate-buffered saline (PBS, from Invitrogen) solution for 30 minutes, followed by rinsing twice with fresh PBS for 5 minutes. C2C12 mouse myoblasts (from the American Type Culture Collection (ATCC) (LOT: 58127344)) were seeded onto the substrate films in 24-well plates at a density of 2.5×10^5 cells per ml and cultured within a standard tissue culture incubator at 37 °C with 7% CO_2. The growth medium (GM) for culturing the C2C12 myoblasts consisted of DMEM (Invitrogen) supplemented with 20% fetal bovine serum (Lot#41F0482K; Invitrogen) and 2 mM L-glutamine (Invitrogen). After incubation of the cells on the substrates for 24 hours, the GM was replaced with 500 μl of MTT reagent (2.5 mg ml^{-1} MTT in PBS; Sigma no. M2128). Following incubation for 3 hours the MTT reagent was replaced by 200 μl dimethyl sulfoxide (DMSO), shielded from light with aluminum foil and placed on a shaker (54 rpm; Stuart, mini gyro-rocker, SSM3) for 10 minutes. Subsequently, 40 μl of solution from each well was transferred into the 96-well plate, mixed with 40 μl DMSO, and the optical density was measured using a microplate reader at a 540 nm wavelength. The tests were done for three time periods, 24 hours, 48 hours and 72 hours.

SEM of cell samples

In order to examine how cells interact with ABFs, C2C12 cells (1×10^5 cells per ml) were seeded onto glass substrates with incorporated arrays of ABFs and incubated in their presence for 24 hours. The cells on the sample were then chemically fixed, dehydrated and dried in a critical point dryer (CPD 030, BAL-TEC) as previously described.[24] Next, a thin film (about 10 nm) of platinum was sputtered onto the sample for SEM inspection (Zeiss ULTRA 55).

Characterization of swimming properties

A Helmholtz coil setup was used to generate uniform rotating magnetic fields, where three orthogonal coil pairs are placed around the experiment tank. More details on the Helmholtz coil setup can be found in previous publications.[19,21] All the tests were conducted on a clean surface of Si in DI-water. The swimming behavior was recorded with a microscope and a camera, which are mounted above the tank. The swimming speed was calculated by dividing the movement distance by time.

Acknowledgements

The authors thank Klaus Marquardt from the University of Zurich for helping with the SEM of cells, Jonas Haggenjos for preparing some flat substrates, and Krzysztof K. Krawczyk for helping with the MTT assay tests. The FIRST lab of ETH Zurich for technical support is appreciated. The research has been funded by the Swiss National Science Foundation (SNSF) Project no. 200021-130069.

References

1 B. J. Nelson, I. K. Kaliakatsos and J. J. Abbott, *Annu. Rev. Biomed. Eng.*, 2010, **12**, 55–85.
2 K. E. Peyer, S. Tottori, F. Qiu, L. Zhang and B. J. Nelson, *Chem.–Eur. J.*, 2013, **19**, 28–38.
3 K. Ishiyama, M. Sendoh and K. I. Arai, *J. Magn. Magn. Mater.*, 2002, **242–245**(Part 1), 41–46.
4 S. Balasubramanian, D. Kagan, C.-M. J. Hu, S. Campuzano, M. J. Lobo-Castañon, N. Lim, D. Y. Kang, M. Zimmerman, L. Zhang and J. Wang, *Angew. Chem.*, 2011, **123**, 4247–4250.
5 D. Kagan, S. Campuzano, S. Balasubramanian, F. Kuralay, G.-U. Flechsig and J. Wang, *Nano Lett.*, 2011, **11**, 2083–2087.
6 W. Xi, A. A. Solovev, A. N. Ananth, D. H. Gracias, S. Sanchez and O. G. Schmidt, *Nanoscale*, 2013, **5**, 1294–1297.
7 L. Zhang, T. Petit, Y. Lu, B. E. Kratochvil, K. E. Peyer, R. Pei, J. Lou and B. J. Nelson, *ACS Nano*, 2010, **4**, 6228–6234.
8 L. Zhang, T. Petit, K. E. Peyer and B. J. Nelson, *Nanomedicine*, 2012, **8**, 1074–1080.
9 T. Petit, L. Zhang, K. E. Peyer, B. E. Kratochvil and B. J. Nelson, *Nano Lett.*, 2012, **12**, 156–160.
10 A. Ghosh and P. Fischer, *Nano Lett.*, 2009, **9**, 2243–2245.
11 G. Zhao, S. Sanchez, O. G. Schmidt and M. Pumera, *Chem. Commun.*, 2012, **48**, 10090–10092.
12 H. C. Berg and R. A. Anderson, *Nature*, 1973, **245**, 380–382.
13 J. J. Abbott, K. E. Peyer, M. C. Lagomarsino, L. Zhang, L. X. Dong, I. K. Kaliakatsos and B. J. Nelson, *Int. J. Robot. Res.*, 2009, **28**, 1434–1447.
14 K. E. Peyer, L. Zhang and B. J. Nelson, *Nanoscale*, 2013, **5**, 1259–1272.
15 S. Tottori, L. Zhang, K. E. Peyer and B. J. Nelson, *Nano Lett.*, 2013, **13**, 4263–4268.
16 D. J. Bell, S. Leutenegger, K. M. Hammar, L. X. Dong and B. J. Nelson, in *Proceedings of the 2007 IEEE International Conference on Robotics and Automation*, 2007, vol. 1–10, pp. 1128–1133.
17 V. Y. Prinz, V. A. Seleznev, A. K. Gutakovsky, A. V. Chehovskiy, V. V. Preobrazhenskii, M. A. Putyato and T. A. Gavrilova, *Phys. E*, 2000, **6**, 828–831.
18 L. Zhang, E. Deckhardt, A. Weber, C. Schonenberger and D. Grutzmacher, *Nanotechnology*, 2005, **16**, 655–663.
19 L. Zhang, J. J. Abbott, L. X. Dong, B. E. Kratochvil, D. Bell and B. J. Nelson, *Appl. Phys. Lett.*, 2009, **94**, 064107.
20 L. Zhang, J. J. Abbott, L. Dong, K. E. Peyer, B. E. Kratochvil, H. Zhang, C. Bergeles and B. J. Nelson, *Nano Lett.*, 2009, **9**, 3663–3667.
21 K. E. Peyer, L. Zhang, B. E. Kratochvil and B. J. Nelson, in *2010 IEEE International Conference on Robotics and Automation*, 2010, pp. 96–101.
22 L. Zhang, K. E. Peyer and B. J. Nelson, *Lab Chip*, 2010, **10**, 2203–2215.
23 K. E. Peyer, L. Zhang and B. J. Nelson, *Appl. Phys. Lett.*, 2011, **99**, 174101.

24 S. Tottori, L. Zhang, F. Qiu, K. K. Krawczyk, A. Franco-Obregón and B. J. Nelson, *Adv. Mater.*, 2012, **24**, 811–816.
25 K. S. Lee, R. H. Kim, D. Y. Yang and S. H. Park, *Prog. Polym. Sci.*, 2008, **33**, 631–681.
26 Y.-L. Zhang, Q.-D. Chen, H. Xia and H.-B. Sun, *Nano Today*, 2010, **5**, 435–448.
27 M. Suter, L. Zhang, E. Siringil, C. Peters, T. Luehmann, O. Ergeneman, K. Peyer, B. Nelson and C. Hierold, *Biomed. Microdevices*, 2013, 997–1003.
28 F. Qiu, L. Zhang, S. Tottori, K. Marquardt, K. Krawczyk, A. Franco-Obregon and B. J. Nelson, *Mater. Today*, 2012, **15**, 463.
29 S. Schlie, A. Ngezahayo, A. Ovsianikov, T. Fabian, H. A. Kolb, H. Haferkamp and B. N. Chichkov, *J. Biomater. Appl.*, 2007, **22**, 275–287.
30 F. Klein, T. Striebel, J. Fischer, Z. X. Jiang, C. M. Franz, G. von Freymann, M. Wegener and M. Bastmeyer, *Adv. Mater.*, 2010, **22**, 868–871.
31 S. H. Yoon, Y. K. Kim, E. D. Han, Y. H. Seo, B. H. Kim and M. R. K. Mofrad, *Lab Chip*, 2012, **12**, 2391–2402.
32 A. Doraiswamy, A. Ovsianikov, S. D. Gittard, N. A. Monteiro-Riviere, R. Crombez, E. Montalvo, W. D. Shen, B. N. Chichkov and R. J. Narayan, *J. Nanosci. Nanotechnol.*, 2010, **10**, 6305–6312.
33 C. Schizas and D. Karalekas, *J. Mech. Behav. Biomed. Mater.*, 2011, **4**, 99–106.
34 A. Doraiswamy, C. Jin, R. J. Narayan, P. Mageswaran, P. Mente, R. Modi, R. Auyeung, D. B. Chrisey, A. Ovsianikov and B. Chichkov, *Acta Biomater.*, 2006, **2**, 267–275.
35 F. Klein, B. Richter, T. Striebel, C. M. Franz, G. v. Freymann, M. Wegener and M. Bastmeyer, *Adv. Mater.*, 2011, **23**, 1341–1345.
36 M. Ermolli, C. Menne, G. Pozzi, M. A. Serra and L. A. Clerici, *Toxicology*, 2001, **159**, 23–31.
37 P. P. Mueller, S. Arnold, M. Badar, D. Bormann, F. W. Bach, A. Drynda, A. Meyer-Lindenberg, H. Hauser and M. Peuster, *J. Biomed. Mater. Res., Part A*, 2012, **100**, 2881–2889.
38 M. Peuster, P. Wohlsein, M. Brugmann, M. Ehlerding, K. Seidler, C. Fink, H. Brauer, A. Fischer and G. Hausdorf, *Heart*, 2001, **86**, 563–569.
39 M. Peuster, C. Hesse, T. Schloo, C. Fink, P. Beerbaum and C. von Schnakenburg, *Biomaterials*, 2006, **27**, 4955–4962.
40 S. L. Tao, K. C. Popat, J. J. Norman and T. A. Desai, *Langmuir*, 2008, **24**, 2631–2636.
41 T. Mosmann, *J. Immunol. Methods*, 1983, **65**, 55–63.
42 L. Kupcsik, *Methods Mol. Biol.*, 2011, **740**, 13–19.
43 A. Abarrategi, M. C. Gutierrez, C. Moreno-Vicente, M. J. Hortiguela, V. Ramos, J. L. Lopez-Lacomba, M. L. Ferrer and F. del Monte, *Biomaterials*, 2008, **29**, 94–102.
44 D. Fischer, Y. Li, B. Ahlemeyer, J. Krieglstein and T. Kissel, *Biomaterials*, 2003, **24**, 1121–1131.
45 S. Sanchez, A. N. Ananth, V. M. Fomin, M. Viehrig and O. G. Schmidt, *J. Am. Chem. Soc.*, 2011, **133**, 14860–14863.
46 K. Ishizaki, Y. Sugita, F. Iwasa, H. Minamikawa, T. Ueno, M. Yamada, T. Suzuki and T. Ogawa, *Int. J. Nanomed.*, 2011, **6**, 2191–2203.
47 M. Moravej, F. Prima, M. Fiset and D. Mantovani, *Acta Biomater.*, 2010, **6**, 1726–1735.
48 A. M. Schmidt and D. S. Azambuja, *Mater. Res.*, 2010, **13**, 45–50.
49 R. Waksman, R. Pakala, R. Baffour, R. Seabron, D. Hellinga and F. O. Tio, *J. Interv. Cardiol.*, 2008, **21**, 15–20.
50 K. E. Peyer, F. Qiu, L. Zhang and B. J. Nelson, in *IEEE/RSJ International Conference on Intelligent Robots and Systems*, IEEE, New York, 2012, pp. 2553–2558.

